ADVANCED MATERIALS TECHNOLOGIES
www.advmattechnol.de

Achieving Multiwavelength Optical Amplification Based on Polymer Waveguides Doped with $NaYF_4$:Er^{3+}, Yb^{3+} Nanoparticles under Commercial and Convenient Led Pumping

Ziyue Lv, Xiaowu Shi, Ce Wang, Baoping Zhang, Daming Zhang, Fei Wang, Xibin Wang, Zhaoqin Zhou, Xingchen Yang, Leiying Ying, Jiyun Zhu, Yuyang Huang, and Dan Zhang**

Relying on a reverse energy transfer mechanism between erbium (Er^{3+}) and ytterbium (Yb^{3+}) ions, optical gains at wavelengths of 1550, 980, and 1067 nm are achieved in $NaYF_4$: Er^{3+}, and Yb^{3+} nanoparticles-doped polymer waveguides under excitation of low-power light-emitting diodes (LEDs) instead of 976 or 1480 nm semiconductor laser as pump sources. The optical gains at 1550, 980, and 1067 nm are demonstrated in five waveguide structures: active-rectangular, evanescent-field with and without an aluminium (Al) reflector, and dual-active hybrid with and without an Al reflector. The maximum relative optical gains of 6.6, 4.0, and 3.8 $dBcm^{-1}$ are realized at 1550, 1067, and 980 nm, respectively, in a 5 mm long dual-active hybrid waveguide with cross-section of 4 × 10 µm, and a ≈100 nm-thick Al reflector grown under the lower cladding layer under excitation of a 395 nm LED. This work proves the feasibility of using a low-cost LED to realize multi-wavelength amplification in a dense wavelength-division multiplexing system and is thus valuable for the development of complex multi-functional photonic-integrated-module mixed-band optical communication systems.

1. Introduction

Erbium (Er^{3+})- and ytterbium (Yb^{3+})-co-doped waveguide amplifiers (EYDWAs) can afford an optical gain of several decibels(dBs) in a centimeter-scale waveguide, which can be integrated with various planar waveguide devices such as modulators, optical switches, couplers, arrayed waveguide gratings, and micro-ring resonators to realize zero net optical loss on-chip optical systems with a wavelength in the C-band.[1–6] Generally, both inorganic and organic host materials doped with Er^{3+} and Yb^{3+} ions can be used to fabricate EYDWAs. Inorganic EYDWAs comprise phosphate,[7,8] silicate,[9–11] $LiNbO_3$ crystals,[12–14] tellurium glass,[15], and Al_2O_3,[16–18] among others. Yang Liu et al. used a 0.5 m long Er:Si_3N_4 waveguide coil to achieve an output power of 145 mW and a small-signal gain of >30 dB, comparable to that of commercial fiber-optic amplifiers.[19] The pertinent inorganic EYDWAs fabrication technologies have been well developed, including ion exchange,[20,21] ion implantation,[22,23] electron beam etching,[24,25] and femtosecond laser writing,[26–28] and so on. Inorganic hosts, in general, allow for high doping concentrations and long excited-state lifetimes (on the order of milliseconds) of Er^{3+} ions, making it relatively effortless to generate high gains (a few dB to several tens of dB) on a cm-long waveguide. However, the disadvantages of high production cost and poor compatibility with silicon substrates limit their application in planar photonic integration. In contrast, polymers have the advantages of an easily adjustable refractive index, high packaging density, low-cost, high flexibility, and simple processing; therefore, have become one of the most popular optical waveguide host materials, and are compatible with various mature substrate materials for fabricating monolithic integrated photonic circuits.[29] Generally, speaking, Er^{3+} ions can be used to synthesize Er complexes with organic ligands, such as $Er(DBM)_3phen$,[30] $Er_{1.2}Yb_{0.8}(PBa)_6(Phen)_2$,[31,32], and $Er(THMD)_3$,[33] or be encapsulated into metal fluoride shells to form core–shell nanoparticles (NPs) with Yb^{3+} ions, such as LaF_3: Er^{3+}, Yb^{3+},[34] $BaYF_5$:Yb^{3+}, Er^{3+},[35] $NaYF_4$: Er^{3+}, Yb^{3+},[36], and then doped in polymer hosts to prepare organic Er^{3+} doped waveguide amplifiers (EDWAs). Compared with Er complexes, the metal fluoride NPs usually exhibit low phonon energy and effective inhibition of concentration quenching, making them the mainstream material for organic EYDWAs. The EYDWAs

Z. Lv, X. Shi, C. Wang, B. Zhang, Z. Zhou, X. Yang, L. Ying, J. Zhu, Y. Huang, D. Zhang
School of Electronic Science and Engineering (National Model Microelectronics College)
Xiamen University
Xiamen 361005, China
E-mail: zhangdan@xmu.edu.cn
D. Zhang, F. Wang, X. Wang
State Key Laboratory of Integrated Optoelectronics
College of Electronic Science and Engineering
Jilin University
2699 Qianjin Street, Changchun 130012, China
E-mail: zhangdm@jlu.edu.cn
The ORCID identification number(s) for the author(s) of this article can be found under https://doi.org/10.1002/admt.202301379

DOI: 10.1002/admt.202301379

require the use of pump sources to achieve energy conversion. Corresponding 976 nm semiconductor lasers can match the intrinsic absorption levels of Er^{3+} ($^4I_{15/2} \rightarrow {}^4I_{11/2}$) and Yb^{3+} ions ($^2F_{7/2} \rightarrow {}^2F_{5/2}$) well, and have the advantages of energy concentration and high photoexcitation efficiency; thus, they are usually chosen as pump sources to excite EYDWAs. Yb^{3+} ions are generally added as sensitizers for Er^{3+} ions because their absorption cross-section ($^2F_{7/2} \rightarrow {}^2F_{5/2}$) at 976 nm is approximately an order of magnitude higher than that of Er^{3+} ions ($^4I_{15/2} \rightarrow {}^4I_{11/2}$),[37] which can help improve the absorption efficiency of the 976 nm pump energy, enhancing the luminescence of Er^{3+} ions at 1550 nm. In the optical coupling mode, a 1550/976 nm wavelength division multiplexer (WDM) is typically incorporated to combine the optical signal laser and pump laser; the combined laser beams can then enter the input side of the waveguide through end-face coupling.[38] Such traditional pumping methods usually employ forward, backward, and bidirectional pumping with high power of 100–400 mW,[39,40] and is commonly adopted for several meter-long Er^{3+}-doped fiber amplifiers with Er^{3+} ions concentration of 10^{24} ions m^{-3}; However, for highly doped EYDWAs constituting 10^{26} ions m^{-3} in a cm-long waveguide, drawbacks arise, such as upconversion luminescence effect of Er^{3+} ions,[41] thermal damage to the waveguide end face,[42] and gain quenching due to the increase in device temperature caused by excessive pump power. Further, the additional loss introduced by the WDM is a negative factor in achieving optical gain. Moreover, semiconductor lasers are expensive; therefore, the use of multiple EYDWAs in a planar photonic dense WDM system will undoubtedly lead to significant additional costs, which are not conducive to large-scale market-oriented production applications.

In our recent study, a polymer waveguide amplifier doped with thermally activated delayed fluorescence molecule $AQ(PhDPA)_2$, which has a strong absorption cross-section at 200–400 nm, enabled the realization of photoluminescence, and optical amplification at 637 nm under the excitation of a low-power light-emitting diode (LED).[43] It will be interesting and pioneering if LEDs can be used to replace traditional semiconductor lasers to realize the optical amplification of EYDWAs. Inspired by this idea, $NaYF_4$:Er^{3+}, Yb^{3+} NPs were selected to prepare polymer EYDWAs. By doping them into polymethylmethacrylate (PMMA) and SU-8 polymers as active materials, five different waveguide structures were designed and fabricated: active-rectangular, evanescent-field, dual-active hybrid, evanescent-field with an aluminium (Al) reflector, and dual-active hybrid with an Al reflector. The optical gains of the Er^{3+} ions at 1550 nm were demonstrated in these waveguides under the excitation of a 395 nm LED. Interestingly, Yb^{3+} ions are no longer used as sensitizers of Er^{3+} ions, but act together with Er^{3+} ions as luminescent central ions, achieving gains at wavelengths of 980 and 1067 nm. To further improve the utilization efficiency of the pump energy in the vertical top-pumping mode of the LED, a ≈100 nm-thick Al film was laid as a reflector, which increased the interaction path between the pump light and the active material. The optical gains at 1550, 980, and 1067 nm wavelengths of the waveguide with Al reflector improved by more than two times compared with the waveguides without reflector. The mechanism of multi-wavelength luminescence between the multiple energy levels of Er^{3+} and Yb^{3+} ions under UV LED excitation is discussed herein.

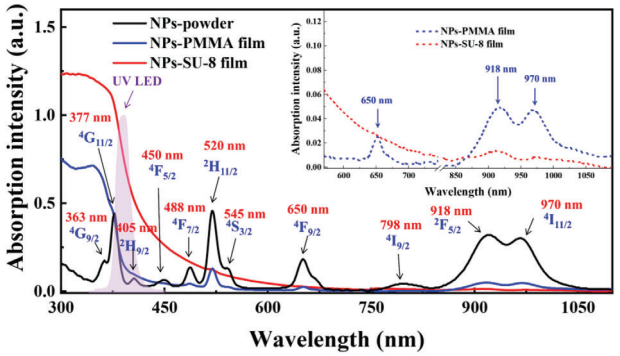

Figure 1. The absorption spectra of $NaYF_4$: Er^{3+}, Yb^{3+} NPs powder and NPs -doped SU-8 and PMMA films.

Relying on the reverse energy transfer mechanism and UV LED top-pumping technology, it is possible to avoid upconversion luminescence effect, thermal damage to the waveguide end face, and gain quenching due to the increase in waveguide temperature caused by high-power pumping of the laser source in polymer EYDWAs. Meanwhile, a coupling packaging for polymer EYDWAs with LED pump sources in planar photonic integrated chips can be easily achieved, which significantly reduce the cost of commercialization. And achieving multi-wavelength amplification in a dense WDM system using a commercial and convenient LED as pump source is of great significance for developing complex multi-functional photonic integrated chips.

2. Experimental Details

2.1. Absorption Properties

The Er^{3+} and Yb^{3+}co-doped sodium yttrium oxyfluoride ($NaY_{1.54}Yb_{0.40}$ $Er_{0.06}$ F_5O) NPs were purchased from Sigma–Aldrich (Shanghai) Trading Co. Ltd. The molar ratio of Er^{3+}:Yb^{3+} is ≈1:7. Two commonly used polymer waveguide materials, SU-8 3005 (Kayaku Advanced Materials, Inc.) and PMMA (Macklin Biochemical Co., Ltd.) were used as the host of $NaYF_4$: Er^{3+}, Yb^{3+} NPs to form active polymers. Here, 0.01 g $NaYF_4$: Er^{3+}, Yb^{3+} NPs was dissolved in 0.2 mL of toluene, and subsequently added to 1 g SU-8 3005 and a solution of 0.6 g PMMA in 2.4 mL n-butyl acetate, respectively. The mixture was put in a glass weighing bottle and stirred at room temperature for 48 h. The doping concentrations of $NaYF_4$: Er^{3+}, Yb^{3+} in SU-8 and PMMA polymer were 1 *wt.*% and 1.67 *wt.*% respectively, which is almost the maximum doping concentration to keep the premise of ensuring the film with lower surface roughness. These two mixed solutions, $NaYF_4$: Er^{3+}, Yb^{3+} NPs-doped SU-8 and -doped PMMA, were heated at 120 °C for 6 h to form films for absorption measurement, with thicknesses of ≈1.04 and 0.35 mm, respectively. The absorption spectra of the $NaYF_4$: Er^{3+}, Yb^{3+} NPs powder and NPs-doped films taken by a SHIMADZU UV-visible spectrophotometer were shown in **Figure 1**. The powder has a strong absorption band in the UV band from 300 to 410 nm, corresponding to the intrinsic transitions of Er^{3+} ions from the ground state $^4I_{15/2}$ to $^4G_{9/2}$ (363 nm), $^4G_{11/2}$ (377 nm), and $^2H_{9/2}$ (405 nm) excited states, and some typical absorption peaks of Er^{3+} ions at 450, 488, 520, 545,

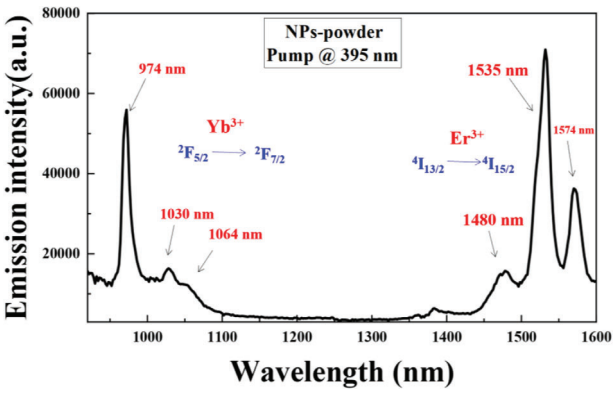

Figure 2. Room temperature near-infrared PL spectrum of $NaYF_4$: Er^{3+}, Yb^{3+} NPs powder under the excitation of 395 nm xenon lamp.

650, and 798 nm, corresponding to transitions from $^4I_{15/2}$ to $^4F_{5/2}$, $^4F_{7/2}$, $^2H_{11/2}$, $^4S_{3/2}$, $^4F_{9/2,}$ and $^4I_{9/2}$ excited states. In the absorption spectrum, the absorption peaks at 918 and 970 nm were caused by the transition of Yb^{3+} ions from the ground state $^2F_{7/2}$ to $^2F_{5/2}$,[44] and the absorption at 970 nm also includes the transition of Er^{3+} ions from $^4I_{15/2}$ to $^4I_{11/2}$. The absorption spectra of $NaYF_4$:Er^{3+}, Yb^{3+} NPs -doped SU-8 and PMMA films were also obtained respectively in Figure 1. The absorption intensity of almost all the intrinsic absorption peaks from 450 to 1000 nm of $NaYF_4$:Er^{3+}, Yb^{3+} NPs was attenuated in the PMMA and SU-8 polymer films because the concentration of Er^{3+} and Yb^{3+} ions in polymer films was much lower compared with that in powder aggregation state. A local magnification of the -doped films was shown in the inset, where the characteristic absorption peaks of Er^{3+} and Yb^{3+} ions at 650, 918, and 970 nm could be seen. Due to the wide and continuous absorption band of $NaYF_4$: Er^{3+}, Yb^{3+} NPs -doped polymers in the range of 300–450 nm, which is mainly caused by the absorption of SU-8 and PMMA,[45] the intrinsic absorption of Er^{3+} ions at $^4G_{9/2}$ (363 nm), $^4G_{11/2}$ (377 nm), and $^2H_{9/2}$ (405 nm) was all covered by this UV absorption band. Owing to the different morphologies, thickness, and doping concentrations of the films and powder, their absorption intensities were not comparable. According to the quantum cutting (QC) process that can split one incident high-energy photon into two or more lower-energy photons with a higher energy conversion efficiency,[46] a UV light source, which could cover the two intrinsic absorption at 377 and 405 nm of Er^{3+} ions could be employed to attempt photoluminescence of $NaYF_4$:Er^{3+}, Yb^{3+} NPs.

2.2. Photoluminescence Properties

Figure 2 shows the photoluminescence (PL) spectrum of the $NaYF_4$: Er^{3+}, Yb^{3+} NPs powder in near-infrared band excited by 395 nm xenon lamp using a steady state and transient fluorescence spectrometer (Edinburgh FLS1000). The PL peaks ≈1535 nm, including 1480 and 1574 nm were the transitions of Er^{3+} ions from excited state $^4I_{13/2}$ to ground state $^4I_{15/2}$, indicating that Er^{3+} ions have achieved population inversion from $^4I_{15/2}$ to $^4G_{11/2}$ and $^2H_{9/2}$ states under excitation of the 395 nm xenon lamp. While the PL peaks at 974,1030, and 1064 nm were due to the transition of Yb^{3+} ions from the excited state $^2F_{5/2}$ to ground state $^2F_{7/2}$. Because Yb^{3+} ions with a single excited $^2F_{5/2}$ state do not directly absorb in the UV and visible light,[47] thus the PL peaks of Yb^{3+} ions at above three near-infrared wavelengths, attributed to the $^2F_{5/2} \rightarrow {}^2F_{7/2}$ transition, were mainly caused by the energy transfer from Er^{3+} to Yb^{3+} ions under 395 nm excitation.

2.3. Feasibility Analysis of Waveguide Fabrication

The doping concentrations have an important influence on the optical gain. In order to produce several dBs of optical gain in a cm-long waveguide, the doping concentration of rare-earth ions in polymer hosts should be as high as possible. However, high concentration easily leads to poor film-formation and concentration quenching, and increase the transmission loss and scattering loss of the waveguide, which is an unfavorable factor for optical gain. **Figure** 3a,b) displays the atomic force microscopy (AFM) micrographs of the $NaYF_4$: Er^{3+}, Yb^{3+} NPs -doped polymer SU-8 (1.0 *wt.*%) and PMMA (1.67 *wt.*%) films, respectively. The doping concentration was consistent with that used to fabricate waveguides. The active films were fabricated by spin coating on Si wafers and thermal curing at 120 °C for 2 h with 4 and 5 μm-thick of $NaYF_4$: Er^{3+}, Yb^{3+} NPs -doped SU-8 and PMMA film respectively. In a 3 × 3 μm range taken for detection, the roughness measurement of the surface was 799.4 and 700.0 pm respectively, which indicates good film quality of $NaYF_4$: Er^{3+}, Yb^{3+} NPs-doped polymers.

The refractive indices of $NaYF_4$: Er^{3+}, Yb^{3+} NPs -doped SU-8 and PMMA were measured by ellipsometry (J.A. Woollam, Co. M2000) at wavelengths of 980, 1067, and 1550 nm, respectively. At these wavelengths, the refractive indices of the NPs -doped SU-8 were 1.578, 1.576, and 1.572, while the refractive indices of the NPs -doped PMMA were 1.494, 1.493, and 1.492, respectively. According to these two active polymers, five kinds of waveguides with different structures were designed, as shown in **Figure** 4a–d). Commercial SU-8 3005 polymer was an epoxy-crosslinkable negative photoresist with good visible transparency and high thermal stability that enables the direct fabrication of the channel waveguides by one-step lithography. Therefore, the rectangular structure of an active SU-8 waveguide, which was commonly used as waveguide structure for the rare-earth ions -doped nanoparticle materials,[48] was designed in Figure 4a). The evanescent-field waveguide[49] with $NaYF_4$: Er^{3+}, Yb^{3+} NPs -doped PMMA as the upper layer, and passive SU-8 or active $NaYF_4$: Er^{3+}, Yb^{3+} NPs -doped SU-8 as channel waveguides were designed respectively, as shown in Figure 4b,c). The amplification principle of this waveguide structure was indicated in Figure 4e). When the optical signal laser propagates in the channel waveguides, the photon energy could enter the active upper cladding in form of evanescent-wave and trigger the stimulated radiation of the rare-earth ions in the upper cladding under the excitation of the pump source. After replacing the passive SU-8 channel waveguide shown in Figure 4b) with the active $NaYF_4$: Er^{3+}, Yb^{3+} NPs -doped SU-8, as shown in Figure 4c), due to the existence of Er^{3+} ions in both core and cladding layers, a better gain effect was expected to be obtained in this dual-active hybrid waveguide.

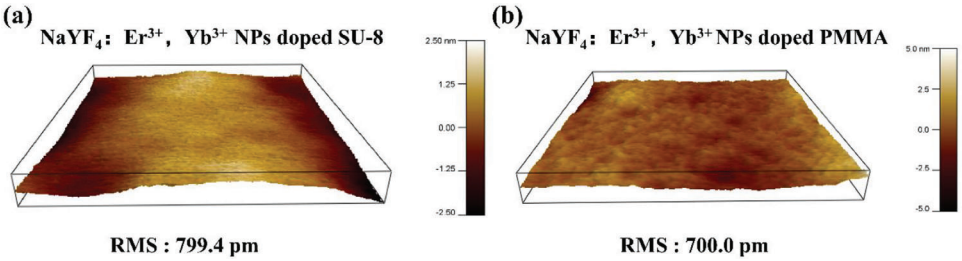

Figure 3. The AFM image of $NaYF_4$: Er^{3+}, Yb^{3+}-doped a) SU-8 film and b) PMMA film, respectively.

In order to improve the utilization efficiency of the radiation of the LED pump light in the vertical direction, a ≈100 nm-thick Al film was grown on silicon substrate as a reflector. Meanwhile, a 4 μm-thick PMMA was spin-coated on the Al reflector as a lower cladding and prevent surface oxidation of Al film. The dual-active waveguide structure with Al reflector was presented in Figure 4d). In addition, Al film was not only introduced into dual-active waveguide, but also added as a reflector in evanescent-field waveguide to compare the gain performance obtained with the structure shown in Figure 4b).

2.4. Waveguide Fabrication

According to the waveguide structures designed in Figure 4, five kinds of waveguides, namely active-rectangular waveguides, evanescent-field waveguides with and without Al reflector, dual-active hybrid waveguides with, and without Al reflector, were fabricated, respectively. First, a ≈4 μm-thick $NaYF_4$:Er^{3+}, Yb^{3+} NPs -doped SU-8 as the core layer was spin-coated onto a silicon substrate with a ≈2 μm-thick SiO_2 as the bottom cladding. A set of waveguides with a width of 10 μm and a height of 4 μm were fabricated by one-step photolithography to form the active-rectangular waveguide. The scanning electron microscope (SEM) micrograph of the active-rectangular waveguide was shown in **Figure** 5a). A group of passive SU-8 3005 channel waveguides with cross-section of ≈4 × 10 μm^2 could be fabricated according to the above process. By spin coating a ≈1.7 μm-thick $NaYF_4$: Er^{3+}, Yb^{3+} NPs -doped PMMA as active upper cladding, the evanescent-field waveguide designed in Figure 4b) could be obtained. The cross-section and top view SEM micrograph of the evanescent-field waveguide was presented in Figure 5b). The dual-active hybrid waveguide designed according to Figure 4c) could be realized by spin coating a ≈2.6 μm-thick $NaYF_4$: Er^{3+}, Yb^{3+} NPs -doped PMMA as active upper cladding on $NaYF_4$:Er^{3+}, Yb^{3+} NPs -doped SU-8 active-rectangular waveguides with

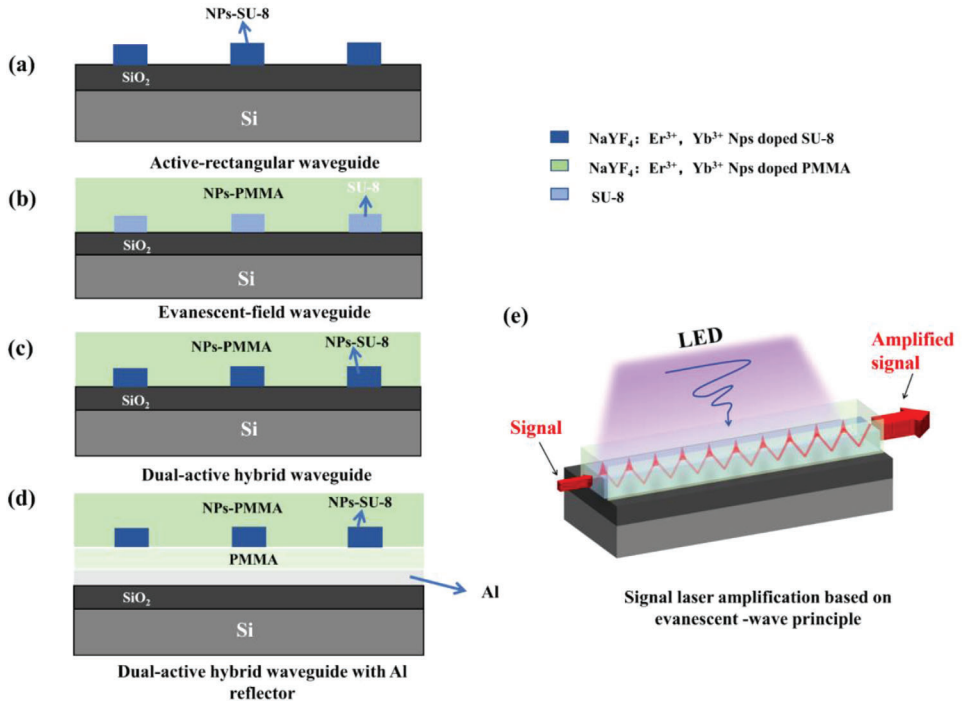

Figure 4. Schematic diagram of waveguides with different structures. a) Rectangular waveguides with $NaYF_4$: Er^{3+}, Yb^{3+} NPs -doped SU-8 as channel waveguides. b) Evanescent-field waveguides with passive SU-8 as channel waveguides and $NaYF_4$: Er^{3+}, Yb^{3+} NPs -doped PMMA as upper cladding. c) Dual-active waveguide structure with $NaYF_4$: Er^{3+}, Yb^{3+} NPs -doped SU-8, and -doped PMMA as active core and upper cladding, respectively. d) Dual-active waveguide structure with a ≈100 nm-thick Al reflector. e) The path of amplified signal laser based on evanescent-wave amplification principle.

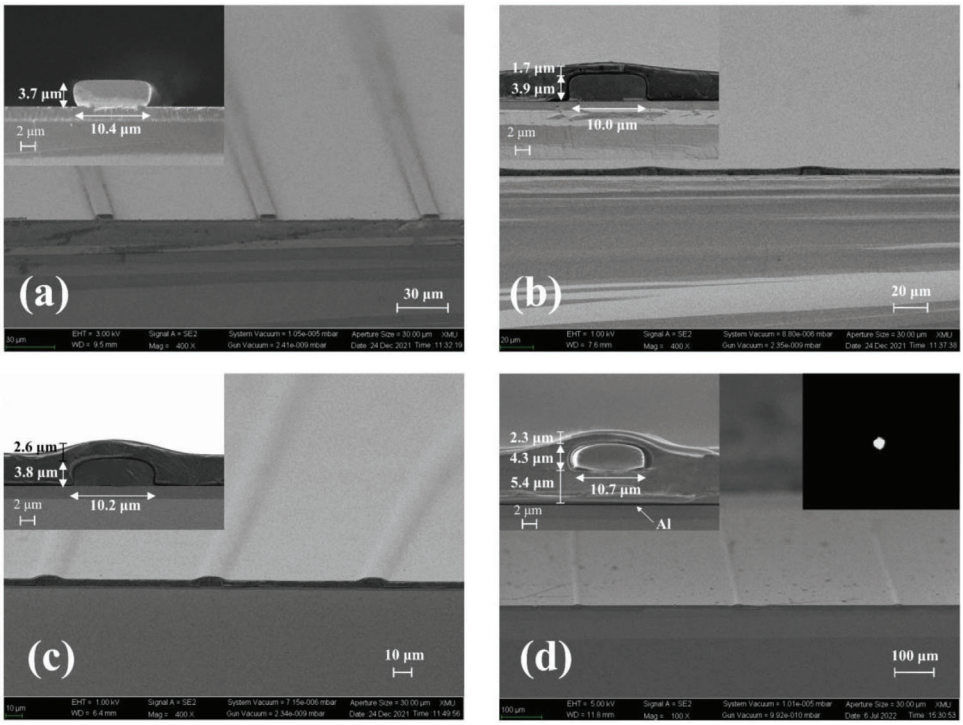

Figure 5. Cross sectional and top view of SEM micrographs of a) $NaYF_4$:Er^{3+}, Yb^{3+} NPs -doped SU-8 active-rectangular waveguides (≈4 × 10 μm). b) Evanescent- field waveguide with SU-8 as channel waveguide with cross-section of ≈4 × 10 μm. The $NaYF_4$: Er^{3+}, Yb^{3+} NPs -doped PMMA was spin-coated as upper cladding (≈1.7 μm-thick on top surface of the waveguide). c) Dual-active waveguide structure with $NaYF_4$: Er^{3+}, Yb^{3+} NPs -doped SU-8, and -doped PMMA as active core and upper cladding, respectively. The cross-section of channel waveguide is ≈4 × 10 μm. The thickness of upper cladding is ≈2.6 μm. d) Dual-active waveguide with a ≈100 nm Al reflector and a ≈5.4 μm-thick PMMA as bottom cladding. The inset is the output near-field profile from a 10 mm-long waveguide at 1550 nm wavelength.

cross-section of ≈4 × 10 μm, as shown in Figure 5c). Figure 5d) presented the SEM micrograph of cross-section view for dual-active hybrid waveguide with Al reflector according to the structural design of Figure 4d). A ≈100 nm-thick Al reflector was sputtered onto the SiO_2 substrate, and then a ≈5.4 μm-thick PMMA polymer was spin-coated between the Al film and the waveguide core layer as the bottom cladding, which can also protect the surface of the Al reflector from being oxidized for a better reflection efficiency. Al reflector, with a mature preparation process and cost-effective features, has a good reflection efficiency up to 90% in the ultraviolet part of UV-LED.[50] The inset of Figure 5d) was the output near-field profile from a 10 mm-long waveguide at 1550 nm wavelength when the input signal power is 0.6 mW. In addition, evanescent-field waveguide with Al reflector was prepared according to the above fabrication technology, including sputtering a ≈100 nm-thick Al film, and spin-coating a ≈5.4 μm-thick PMMA as the lower cladding.

2.5. Optical Gain Properties

An experimental setup that can realize amplification of 1550, 980, and 1067 nm wavelengths by LED pumping was established, as shown in **Figure 6**. Three signal lasers at 980 nm (0–10 mW, Lumentum, Tailand, and S27-UGC281 S27-7402-360-ALRoHS), 1067 nm (0–3 mW, Leishi, Changchun, China, MW-SGX-635, and MW-IR-1060), and 1550 nm (0–3 mW, Conquer, Beijing, and China KG-DFB-15-10-SM-FA) were used as the signal sources, respectively and an LED (0–300 mW, YL-UVAHP-6060-405, and UVSIS) with a central wavelength of 395 nm and covering the 360–430 nm band, overlapping two intrinsic absorption at 377 and 405 nm of Er^{3+} ions was selected as the pump source. The radiation spectrum of LED was inserted in Figure 1. The LED was placed ≈5 mm above the polymer waveguide. The viewing angle of the LED was ≈90°. Based on the irradiation intensity distribution, ≈80% of the energy could be concentrated in the area of 1 cm^2, which almost completely covered the areas of a 1 cm-long waveguide device. When the power of the LED was 278 mW, the power available on the waveguide device was ≈222 mW. The signal lasers I_o of the three wavelengths were input through the end coupling of single-mode fibers and waveguides, respectively.

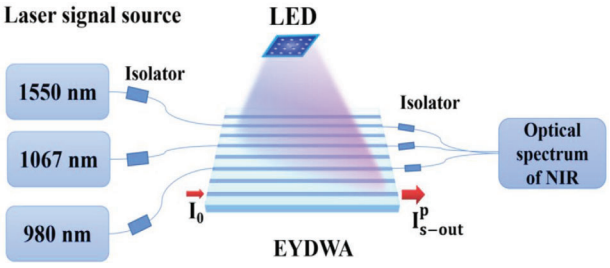

Figure 6. Experimental setup for optical gain measurement of polymer waveguides using vertical top-pumping LED mode.

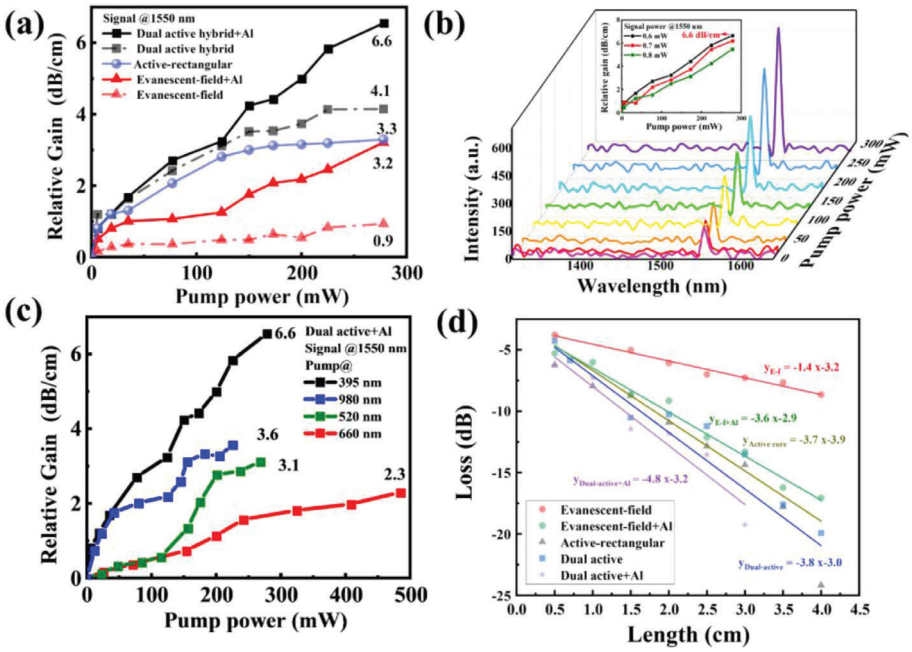

Figure 7. a)The relative gain at 1550 nm as a function of pump power in five different structures of waveguides. b) The relationship between the output signal intensity P^{p}_{s-out} at 1550 nm with the increase of pump power based on dual-active hybrid waveguides with Al reflector under excitation of a 395 nm LED. The inset indicates relative gains as a function of pump power with different input signal powers under excitation of the 395 nm LED. c)The relative gain at 1550 nm as a function of pump power pumping by different LEDs at 395, 520, 660, and 980 nm. d) Loss of five waveguides testing by cut-back method at 1550 nm.

The output signals under the pump excitation I^{p}_{s-out} were coupled to the spectrometer (Ocean Optics FLAME-NIR-INTSMA25) by three single-mode fibers with isolator, respectively. The unity relative gain G_{rel} was defined as the formula,[51]

$$G_{rel}\,(dB/cm) = 10lg\left(\frac{P^{p}_{s-out}}{P_{s-out}}\right)/L \quad (1)$$

where P^{p}_{s-out} and P_{s-out} were the powers of the output signal laser with and without pump power as measured by spectrometer respectively. L was length of the waveguide.

Due to different designs of waveguide structures, the propagation losses of these waveguides also vary. To ensure stable output light intensity and reduce gain fluctuation noise, waveguides with different lengths were fabricated and selected. The lengths L were 7, 20, and 5 mm corresponding to active-rectangular waveguide, evanescent-field waveguide, and dual-active hybrid waveguide, respectively. And the lengths L of the evanescent-field waveguide and dual-active hybrid waveguide with Al reflectors were 10 and 5 mm, respectively. Because the linear increase of relative optical gain with the waveguide length within the range of 5–20 mm, it does not affect the comparison of gain performance obtained per unit length for these waveguides with different lengths.

3. Results and Discussion

Figure 7a) presents the relative gain measurement results based on aforementioned different structures of the waveguides at 1550 nm. The output signal power was 0.6 mW. Under the excitation of the 395 nm LED with power of 278 mW, the relative gain could reach 6.6, 4.1, 3.3,3.2, and 0.9 dBcm^{-1} at the structure of dual-active hybrid waveguide with Al reflector, dual-active hybrid waveguide, active-rectangular waveguide, evanescent-field waveguide with Al reflector, and evanescent-field waveguide, respectively. The evanescent-field waveguide that comprises a passive core and an active upper cladding showed the lowest relative gain value among these waveguides, due to only ≈3,4% of the signal laser penetrates through the channel waveguide and causes stimulated radiation of the active material in the upper cladding. A higher gain value of 4.1 dBcm^{-1} was obtained in the dual-active hybrid waveguide, which was almost equal to the sum of the gain values of the active-rectangular (3.3 dBcm^{-1}) and evanescent-field waveguides (0.9 dBcm^{-1}). This is because the dual active layer makes the active material providing gain almost equivalent to the superposition of two separate single active layers. In addition, with the help of Al reflector, the utilization efficiency of the radiation from the LED pump light in the vertical direction can be enhanced. This subsequently leads to an improvement in the relative gain of the waveguide without any increase in pump power. With the addition of the Al reflector, the evanescent-field waveguide and dual-active hybrid waveguide achieved gains that were 3.6 times greater, increasing from 0.9 to 3.2 dB cm^{-1} and 1.6 times greater, increasing from 4.1 to 6.6 dB cm^{-1} respectively, when the pump power was maintained at 278 mW.

Among these waveguides, the dual-active hybrid waveguide with Al reflector exhibited the best relative gain performance. The variation process of output signal intensity P^{p}_{s-out} measured by spectrometer with the increase of pump power was shown in

Table 1. The propagation loss α_{loss}, relative gain G_{rel}, and internal gain G_{int} at 1550 nm for five different waveguides.

Waveguide type	Propagation loss[dB cm^{-1}]	G_{rel} [dBcm^{-1}]	G_{int} [dBcm^{-1}]
Active-rectangular waveguide	3.7	3.3	−0.4
Evanescent-field waveguide (without Al / with Al)	1.4 / 3.6	0.9 / 3.2	−0.5 / −0.4
Dual-active hybrid waveguide (without Al / with Al)	3.8 / 4.8	4.1 / 6.6	0.3 / 1.8

Figure 7b). Relative gain of 6.6 dB cm^{-1} was obtained at 1550 nm under the 395 nm LED pumping (278 mW). For a fixed pump power, the gain value decreased marginally with an increase of the input signal power, as indicated in the insets of Figure 7b). The maximum gain value decreased from 6.6 to 5.5 dBcm^{-1} as the signal power increased from 0.6 to 0.8 mW for the pump power of 278 mW. This is because a higher signal power will cause a greater consumption of n_2 and a lower reverse population density Δn, which is defined as $\Delta n = n_2 - n_1$, where n_2 and n_1 are the population numbers of Er^{3+} ions in the sub-stable and ground states, respectively. And the Δn is proportional to the gain coefficient g, which represents the relative increase rate of the input signal passing through the unit-length waveguide. Thus, the higher the signal power, the lower the Δn and g.

The absorption spectrum of $NaYF_4$:Er^{3+}, Yb^{3+} NPs -doped polymer film showed three additional absorption cross-sections at 520, 650, and 970 nm, as illustrated in Figure 1. To compare gain performance, three LEDs were selected as pump sources with central wavelengths of 520, 660, and 980 nm, covering the ranges of 480–580, 620–680, and 930–1050 nm, respectively, as shown in Figure 7c). For the dual-active hybrid waveguide with Al reflector, maximum gains of 3.6, 3.1, and 2.3 dB cm^{-1} were observed under the excitation of 980, 520, and 660 nm LED, respectively. The signal power kept 0.6 mW at 1550 nm. These values were all less than the 6.6 dB cm^{-1} obtained by 395 nm LED pumping with approximately the same excitation power. The gain value was lowest when using 660 nm LED pumping due to the smallest absorption cross-section at 660 nm for $NaYF_4$:Er^{3+}, Yb^{3+} NPs -doped polymer film. While the irradiation spectrum of 395 nm LED contains two intrinsic absorption peaks of Er^{3+} ions at 377 and 405 nm, resulting in the best pumping effect. For the aforementioned five different structures of the waveguides, the propagation losses α_{loss} and coupling loss at 1550 nm were measured by the cutback method, as shown in Figure 7d). Of these waveguides, those containing active material in the core layer, such as active-rectangular, and dual-active hybrid waveguides, exhibit relatively high propagation losses, with values of ≈3.7 and 3.8 dB cm^{-1}, respectively. This is due to the absorption and scattering losses caused by $NaYF_4$:Er^{3+}, Yb^{3+} NPs present in the channel waveguides. The evanescent-field waveguide has a relatively small propagation loss of ≈1.4 dB cm^{-1} because the optical field is mostly transmitted along the passive SU-8 channel waveguides, which have a cross-section of 4 × 10 μm. The coupling losses of these waveguides were ≈2.0 dB facet^{-1} (see supplementary document S1 for detailed data). Adding Al reflectors to waveguides not only increases the relative gain, but also increases propagation losses, as shown in **Table 1**. The internal gain G_{int} was calculated in Table 1 according to the relationship between the relative gain $G_{rel}$and propagation loss α_{loss} and internal gain $G_{int} = G_{rel} - \alpha_{loss}$.

Among these waveguides, G_{int} in the dual-active hybrid waveguide and dual-active hybrid waveguide with Al reflector were 0.3 and 1.8 dB cm^{-1}, respectively, while the value of G_{int} in other waveguides were negative, which indicates that the optical loss was greater than the gain generated in the waveguide. For dual-active hybrid waveguides with Al reflector, the $NaYF_4$:Er^{3+}, Yb^{3+} NPs contained in the upper cladding and channel waveguide can be secondary excited by vertically incident and reflected LED light. This waveguide structure not only increases the content of active substances, but also improves the efficiency of pump light utilization, thereby achieving better gain performance.

Although the internal gain of these waveguides is not yet ideal, this work provides a solution for improving the gain of active-rectangular and evanescent-field waveguide structures that are commonly adopted in polymer EYDWA research. Furthermore, by optimizing the cross-sectional dimensions of the waveguide to adjust the optical field energy distribution of the signal laser in the core and active upper cladding, the overlap between the pump light and the signal laser could be effectively improved. Therefore, the gain of the dual-active hybrid waveguide is expected to be further increased.

According to the near-infrared PL spectra, optical amplification at 1067 and 980 nm could also be obtained in these waveguides, respectively. When the output signal laser was 0.2 mW at 1067 nm and the pump power of 395 nm LED kept at 278 mW, the relative gain of 4.0/ 3.4, 2.7, and 2.5/ 0.8 dBcm^{-1} at the waveguide structure of dual-active hybrid waveguide with/without Al reflector, active-rectangular waveguide, and evanescent-field waveguide with/without Al reflector, respectively, as shown in **Figure 8a**). When the wavelength of the output signal laser changed to 980 nm with the power of 3 mW, the relative gain of 3.8/ 2.2, 2.0 and 1.8/ 0.7 dBcm^{-1} were achieved in the aforementioned five different waveuguides under the same power LED pumping. The original measurement data of five types of waveguides at the wavelength of 1550, 1067, and 980 nm can be found in the supplementary document S1.

The multiwavelength gain derived from the population inversion of Er^{3+} and Yb^{3+} ions and their transition emissions between multiple energy levels are depicted in **Figure 9**. In contrast to the well-known up-conversion energy transfer process under 976 nm LED excitation, the main energy transfer under 395 nm LED excitation originates from a downshift transition, which is a single-photon process. There is also a more complex energy level jump in the corresponding structure of multi-ion co-doping. The quantum cutting (QC) process is well established and can split one incident high-energy photon into two or more lower-energy photons with a higher energy conversion efficiency.[46] The energy-level structure diagram of Er^{3+} ions under excitation of 395 nm LED is shown in Figure 9a). Er^{3+} ions in the ground state $^4I_{15/2}$ can be excited to $^2H_{9/2}$ by ground state absorption (GSA), and then, through the non-radiative transition (NRT) process, jump from $^2H_{9/2}$ to $^4F_{7/2}$ state. On the one hand, through the NRT process ($^4F_{7/2} \rightarrow {}^4I_{13/2}$) and one radiative transition (RT) process ($^4I_{13/2} \rightarrow {}^4I_{15/2}$),[52] the luminescence of 1550 nm can be achieved, as shown by processes ① and ⑤ in

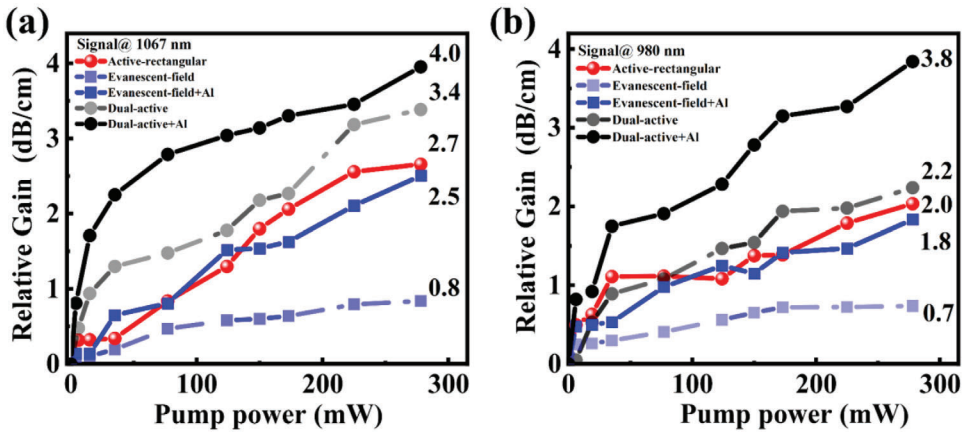

Figure 8. Relative gain performance as a function of pump power at a) 1067 and b) 980 nm in five different structures with the pumping at 395 nm LED with 278 mW.

Figure 9a). On the other hand, after two NRT processes ($^4F_{7/2} \rightarrow {}^2H_{11/2}$) and ($^2H_{11/2} \rightarrow {}^4F_{9/2}$),[53] a cross-relaxation energy transfer occurred between two Er^{3+} ions, as shown in process ②. Through $Er_1^{3+}(^4F_{9/2}) + Er_2^{3+}(^4I_{15/2}) \rightarrow Er_1^{3+}(^4I_{13/2}) + Er_2^{3+}(^4I_{11/2})$, the energy absorbed by the first Er_1^{3+} ion can reach $^4I_{13/2}$ and could achieve the RT process ($^4I_{13/2} \rightarrow {}^4I_{15/2}$). Meanwhile, the second Er_2^{3+} ions on the $^4I_{11/2}$ energy level can continue to transition to the $^4I_{13/2}$ state through the continuous NRT process and achieve the RT process from the $^4I_{13/2}$ to $^4I_{15/2}$ state to realize 1550 nm luminescence. There are also two other cross-relaxation energy transfer processes between the two Er^{3+} ions at the $^2H_{11/2}$ energy level: One is the path of $Er_1^{3+}(^2H_{11/2}) + Er_2^{3+}(^4I_{15/2}) \rightarrow Er_1^{3+}(^4I_{9/2}) + Er_2^{3+}(^4I_{13/2})$,[47] and the other is $Er_1^{3+}(^2H_{11/2}) + Er_2^{3+}(^4I_{15/2}) \rightarrow Er_1^{3+}(^4I_{11/2}) + Er_2^{3+}(^4I_{11/2})$,[48] indicated as processes ③ and ④ in Figure 9a). These cross-relaxation processes resulted in the emission of two photons at 1550 nm via RT process ($^4I_{13/2} \rightarrow {}^4I_{15/2}$). This can be referred to as the near-infrared QC process, which is caused by resonance energy transfer between two Er^{3+} ions. It is well known that Yb^{3+} ions with a single excited $^2F_{5/2}$ state have no direct absorption in the UV and visible ranges.[48] Thus, optical gains at 980 and 1067 nm were obtained in the active waveguides, attributed to the $^2F_{5/2} \rightarrow {}^2F_{7/2}$ transition of Yb^{3+} ions, mainly because of the mechanism of energy transfer from Er^{3+} to Yb^{3+} ions under excitation at 395 nm LED, as presented in Figure 9b). After the GSA process of Er^{3+} ions from the $^4I_{15/2}$ to $^2H_{9/2}$ state, and then through two NRT processes ($^4F_{7/2} \rightarrow {}^2H_{11/2}$) and ($^2H_{11/2} \rightarrow {}^4F_{9/2}$), two cross-relaxation energy transfer processes, also known as QC processes, between Er^{3+} and Yb^{3+} ions could occur. The $^2F_{5/2}$ state of Yb^{3+} ions was populated by the paths of $Er^{3+}(^2H_{11/2}) + Yb^{3+}(^2F_{7/2}) \rightarrow Er^{3+}(^4I_{11/2}) + Yb^{3+}(^2F_{5/2})$ and $Er^{3+}(^4F_{9/2}) + Yb^{3+}(^2F_{7/2}) \rightarrow Er^{3+}(^4I_{13/2}) + Yb^{3+}(^2F_{5/2})$,[48] as shown in processes ⑥ and ⑦ in Figure 9b). In research on the luminescence mechanism of traditional EYDWA, with the pumping of a 976 nm semiconductor laser, Yb^{3+} ions in $^2F_{5/2}$ state could transfer the absorbed near-infrared energy to Er^{3+} ions, help to achieve the luminescence of Er^{3+} ions at 1550 nm. While in this work, the synchronous luminescence process of the two near-infrared wavelengths at 980 and 1067 nm that is illustrated as process ⑧, depends on the reverse energy transfer process from Er^{3+} to

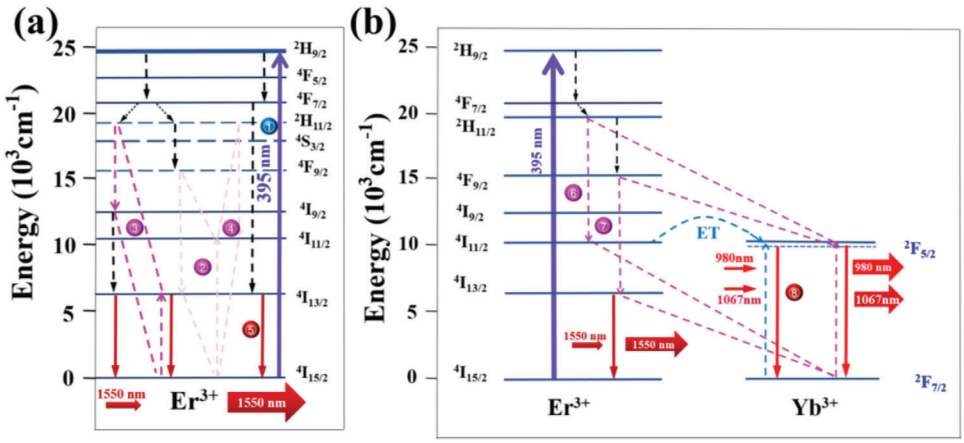

Figure 9. Schematic partial energy-level diagrams of a) Er^{3+} ions; b) The energy transfer mechanism between Er^{3+} and Yb^{3+} ions under the excitation of the 395 nm LED.

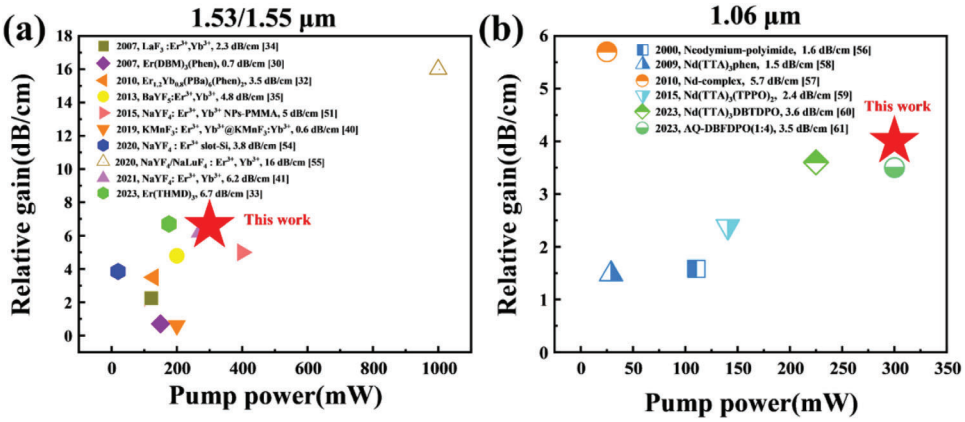

Figure 10. Summary of relative gains of the representative polymer optical waveguide amplifiers gains at 1.53/1.55 and 1.06 μm in recent years.

Yb^{3+} ions when pumped by the UV LED. This luminescence mechanism is significantly different from the traditional energy transfer process of Yb^{3+} to Er^{3+} ions.

To the best of our knowledge, the majority of the previous studies conducted on polymer waveguide amplifiers reported relative gain values of ≈6.0 and ≈4.0 $dBcm^{-1}$ at near-infrared wavelengths using semiconductor lasers as pump sources, as indicated in **Figure 10**.[54–61] The relative gain results of 6.6 and 4.0 $dBcm^{-1}$ at 1550 and 1067 nm based on the dual-active waveguide with Al reflector are higher than the average, and the gain of 3.8 $dBcm^{-1}$ at 980 nm is one of the few reports. It is worth noting that the best reported result of polymer EDWAs at 1535 nm is that a high gain of 16 dB cm^{-1} was achieved when pumped at the 980 nm laser with power of 1000 mW, which may pose a risk of thermal damage to the waveguide end face and shortened service life.[42] Moreover, these polymer waveguide amplifiers focus on optical amplification of a single wavelength. In this work, the LED top-pumping method allowing a single waveguide to carry a smaller pump power density leads to less risk of damage and a longer usage life. The polymer host materials PMMA and SU-8 have been industrially applied in the field of plastic optical fiber and planar photonic integration and proven by the market. When fabricating SU-8 polymer waveguides, it is necessary to ensure sufficient exposure time under UV light to release the photoacid generator in SU-8, thus the impact of UV degradation in SU-8 polymer on the stability of the output signal laser can be basically ruled out. After packaging, the relative gains have been maintained for 6 months without decay at room temperature. The long-term reliability of the device will be further verified in the following research.

4. Conclusion

In summary, we proposed a method to achieve multiwavelength optical amplification based on $NaYF_4$:Er^{3+}, Yb^{3+} NPs-doped polymer waveguides under excitation of a commercial and convenient LED pumping. Five types of waveguides based on $NaYF_4$:Er^{3+}, Yb^{3+} NPs -doped SU-8, and PMMA polymer were designed and fabricated. The absorption and photoluminescence spectra of the active materials were obtained. Under the excitation of 278 mW 395 nm LED, the relative gain at 1550 nm could reach 4.1, 3.3, and 0.9 $dBcm^{-1}$ in dual-active hybrid waveguide, active-rectangular waveguide, and evanescent-field waveguide, respectively. Adding Al reflectors to evanescent-field waveguide and dual-active hybrid waveguide can obviously improve gain from 0.9 to 3.2 dB cm^{-1} and 4.1 to 6.6 dB cm^{-1}, respectively. The relative gains could also be obtained of 4.0/ 3.4, 2.7, and 2.5/ 0.8 $dBcm^{-1}$ (at 1067 nm) and 3.8/ 2.2, 2.0 and 1.8/ 0.7 $dBcm^{-1}$ (at 980 nm) based on the waveguide of dual-active hybrid waveguide with/without Al reflector, active-rectangular waveguide, and evanescent-field waveguide with/without Al reflector, respectively. Using the cutback method, the measured propagation losses of aforementioned five different waveguides were ≈4.8 / 3.8, 3.7, and 3.6 /1.4 dB cm^{-1} at 1550 nm, respectively. Accordingly, the internal gains of 1.8/ 0.3, −0.4, and −0.4/ −0.5 dB cm^{-1} were achieved respectively. Dual-active hybrid waveguide with Al reflector can not only increase the content of active material in the waveguide, but also effectively improve the efficiency of pump light utilization, thereby achieving better gain performance among these waveguides. This work provides a solution for improving the gain of active-rectangular and evanescent-field waveguide structures that are commonly adopted in polymer EYDWAs. In addition, the reverse energy transfer mechanism of multi-wavelength luminescence between the multiple energy levels of Er^{3+} and Yb^{3+} ions under the UV LED excitation was discussed. Different from the energy transfer process of Yb^{3+} to Er^{3+} ions under traditional 980 nm laser pumping, the quantum cutting process established in this work can split one incident high-energy photon into two or more lower-energy photons with a higher energy conversion efficiency.

Relying on the reverse energy transfer mechanism from Er^{3+} to Yb^{3+} ions and UV LED top-pumping technology, it is possible to prevent upconversion luminescence effect, thermal damage to the waveguide end face, and gain quenching due to the increase in waveguide temperature caused by high-power pumping from the laser source. And low-cost coupling packaging of polymer EYDWAs with LED pump source in planar photonic integrated chips can be easily achieved, which can significantly reduce the cost of commercialization. Meanwhile, achieving multi-wavelength amplification in dense WDM system is of great significance for the development of complex multi-functional photonic integrated chips.

Supporting Information

Supporting Information is available from the Wiley Online Library or from the author.

Acknowledgements

This work was supported by the National key research and development plan (No.2021YFB2800500), Natural Science Foundation of Fujian Province of China (No.2022J01063), and National Natural Science Foundation of China (No. 61875170).

Conflict of Interest

The authors declare no conflict of interest.

Data Availability Statement

The data that support the findings of this study are available from the corresponding author upon reasonable request.

Keywords

LED pumping, multiwavelength amplification, $NaYF_4$:Er^{3+},Yb^{3+} nanoparticles, optical gain, polymer waveguide amplifier

Received: August 29, 2023
Revised: December 20, 2023
Published online:

[1] F. Zhao, Q. Bian, Y. Chu, Y. Zhang, Q. Zhao, J. Sun, C. Li, *Phys. Status Solidi RRL.* **2022**,*16*, 2100517.
[2] D. Benedicto, A. Días, J. C. Martín, J. A. Vallés, *J. Lightwave Technol.* **2021**,*39*, 5061.
[3] N. U. Wetter, D. S. da Silva, L. R. P. Kassab, E. Jimenez-Villar, *J. Alloys Compd.* **2019**,*794*, 120.
[4] G. C. Xing, M. L. Zhang, T. H. Sun, Y. W. Fu, Y. L. Huang, J. Shao, J. R. Liu, F. Wang, D. M. Zhang, *Chin. Phys. B.* **2018**, *27*, 114218.
[5] X. Zhang, J. Yan, C. Wang, T. Sun, Z. Cao, C. Xu, G. Qin, F. Wang, D. Zhang, *J. Lightwave Technol.* **2021**,*39*, 3201.
[6] C. Grivas, M. Pollnau, *Laser Photonics Rev.* **2012**,*6*, 419.
[7] J. Hoyo, V. Berdejo, T. T. Fernandez, A. Ferrer, A. Ruiz, J. Valles, M. Rebolledo, I. Ortega-Feliu, *Laser Phys. Lett.* **2013**,*10*, 105802.
[8] W. Wang, G. Yu, S. Lai, C. Jiang, *OSA Continuum.* **2019**,*2*, 1773.
[9] J. Lee, J. H. Shin, N. Park, *J. Lightwave Technol.* **2005**,*23*, 19.
[10] R. M. Guo, B. Wang, X. J. Wang, L. Wang, L. J. Jiang, Z. P. Zhou, *Opt. Lett.* **2012**,*37*, 1427.
[11] S. A. Vázquez-Córdova, M. Dijkstra, E. H. Bernhardi, F. Ay, K. Wörhoff, J. L. Herek, S. M. García-Blanco, *Opt. Express.* **2014**,*22*, 25993.
[12] J. Zhou, Y. Liang, Z. Liu, W. Chu, H. Zhang, D. Yin, Z. Fang, R. Wu, J. Zhang, W. Chen, *Laser Photonics Rev.* **2021**,*15*, 2100030.
[13] S. Suntsov, C. E. Rüter, D. Kip, *Appl. Phys. B: Lasers Opt.* **2017**,*123*, 118.
[14] K. Ahmadi, A. Zakery, *Appl. Phys. B: Lasers Opt.* **2021**,*127*, 67.
[15] V. A. G. Rivera, E. F. Chillcce, E. Rodriguez, C. L. Cesar, L. C. Barbosa, *J. Non-Cryst. Solids.* **2006**,*352*, 363.
[16] J. Bradley, L. Agazzi, D. Geskus, F. Ay, K. Wörhoff, M Pollnau, *J. Opt. Soc. Am. B.* **2010**,*27*, 187.
[17] D. B. Bonneville, H. C. Frankis, R. J. Wang, J. D. B. Bradley, *Opt. Express.* **2020**,*28*, 30130.
[18] J. Rönn, W. W. Zhang, A. Autere, X. Leroux, L. Pakarinen, C. Alonso-Ramos, A. Säynätjoki, H. Lipsanen, L. Vivien, E. Cassan, Z. P. Sun, *Nat. Commun.* **2019**,*10*, 432.
[19] Y. Liu, Z. R. Qiu, X. R. Ji, A. Lukashchuk, J. J. He, J. Riemensberger, M. Hafermann, R. N. Wang, J. Q. Liu, C. Ronning, T. J. Kippenberg, *Science.* **2022**,*376*, 1309.
[20] G. L. C. Rodrigues, T. G. de Oliveira, S. B. S. Gusmao, O. P. Ferreira, T. L. Vasconcelos, Y. Guerra, R. Milani, R. Peña-Garcia, B. C. Viana, *Materials.* **2023**,*16*, 1842.
[21] Y. L. Hao, J. W. Liu, L. F. Che, S. Y. Wang, H. R. Meng, X. Y. Liu, *IEEE Photonics Technol. Lett.* **2023**,*35*, 793.
[22] L. L. Wang, X. J. Cui, N. Q. Liu, *Mod. Phys. Lett. B.* **2018**,*32*, 1850288.
[23] G. Fu, K. M. Wang, X. L. Wang, F. Lu, Q. M. Lu, D. Y. Shen, H. J. Ma, R. Nie, *Surf. Coat. Technol.* **2007**,*201*, 5427.
[24] Y. Zheng, P. P. Gao, X. Tang, J. Z. Liu, J. A. Duan, *J. Cent. South Univ.* **2022**,*29*, 3335.
[25] C. W. Hsu, H. L. Chen, W. C. Chao, W. S. Wang, *Microw. Opt. Technol. Lett.* **2004**,*42*, 208.
[26] Y. J. Xiong, S. X. Wang, Z. X. Chen, X. L. Sun, H. L. Liu, Y. C Jia, F. Chen, *Opt. Laser Technol.* **2023**,*167*, 109786.
[27] R. Li, W. J. Nie, Q. M. Lu, C. Cheng, Z. Shang, J. R. V. de Aldana, F. Chen, *Opt. Laser Technol.* **2017**,*92*, 163.
[28] F. D. Ince, Y. Morova, U. Yazlar, A. Sennaroglu, *Diamond Relat. Mater.* **2023**,*135*, 109894.
[29] J. S. Chang, S. C. Eom, G. Y. Sung, J. H. Shin, *Opt. Express.* **2009**,*17*, 22918.
[30] D. M. Zhang, C. Chen, X. Sun, Y. G. Zhang, X. Z. Zhang, A. H. Wu, B. Li, D. M. Zhang, *Opt. Commun.* **2007**,*278*, 90.
[31] C. Chen, D. Zhang, T. Li, D. M. Zhang, L. M. Song, Z. Zhen, *Appl. Phys. Lett.* **2009**,*94*, 041119.
[32] C. Chen, D. Zhang, T. Li, D. M. Zhang, L. M. Song, Z. Zhen, *J. Nanosci. Nanotechnol.* **2010**,*10*, 1947.
[33] J. Y. Zhu, B. P. Zhang, Y. Y. Huang, Z. Y. Lv, L. Y. Ying, Y. Mei, Z. W. Zheng, D. Zhang, *Opt. Express.* **2023**,*31*, 5242.
[34] D. Zhang, C. Chen, C. M. Chen, C. S. Ma, D. M. Zhang, S. Bo, Z. Zhen, *Appl. Phys. Lett.* **2007**,*91*, 161109.
[35] X. Zhai, S. Liu, X. Liu, F. Wang, D. Zhang, G. Qin, W. Qin, *J. Mater. Chem. C.* **2013**,*1*, 1525.
[36] T. H. Sun, Y. W. Fu, X. C. Zhang, J. M. Yan, F. Wang, D. M. Zhang, *Opt. Commun.* **2021**,*488*, 126723.
[37] M. Zhang, G. Hu, S. Zhang, D. Gao, Y. Sun, F. Wang, *RSC Adv.* **2020**,*10*, 11148.
[38] G. F. R. Chen, X. Y. Zhao, Y. Sun, C. B. He, M. C. Tan, D. T. H. Tan, *Sci. Rep.* **2017**,*7*, 3366.
[39] S. Suntsov, C. E. Rüter, D. Kip, *Appl. Phys. B: Lasers Opt.* **2017**, *123*, 1.
[40] Y. L. Zhang, P. Lv, D. X. Wang, Z. K. Qin, F. Wang, D. M. Zhang, D. Zhao, G. S. Qin, W. P. Qin, *Nanomaterials.* **2019**,*9*, 463.
[41] T. Sun, Y. Fu, Z. Cao, S. Tao, J. Yan, D. Zhao, D. Zhang, F. Wang, D. Zhang, *Opt. Lett.* **2021**,*46*, 5385.
[42] N. N. H. Saris, Y. Yoshida, T. Horie, A. Hamzah, S. Ambran, O. Mikami, T. Ishigure, T. Fukui, *Optik.* **2021**,*239*, 166670.
[43] C. Wang, X. Liu, B. Zhang, G. Xie, Z. Zhou, X. Yang, L. Ying, Y. Mei, W. Fan, Z. Lin, *Adv. Opt. Mater.* **2022**,*10*, 2200205.
[44] W. Fan, B. Zhang, C. Wang, L. Ying, X. Yang, Z. Zhou, D. Zhang, *Opt. Express.* **2021**,*29*, 11372.
[45] G. Rudko, A. Kovalchuk, V. Fediv, W. M. Chen, I. A. Buyanova, *Nanoscale Res. Lett.* **2015**, *10*, 1.
[46] X. Huang, S. Han, W. Huang, X. Liu, *Chem. Soc. Rev.* **2013**,*42*, 173.
[47] Z. Yang, J. Yang, J. Qiu, Z. Song, *Phys. Chem. Chem. Phys.* **2017**,*19*, 31997.

[48] X. Liu, X. Chen, X. Zhai, G. Qin, W. Qin, F. Wang, D. Zhang, *J. Nanosci. Nanotechnol.* **2014**,*14*, 3499.
[49] G. Buse, E. Preda, M. Stef, I. Nicoara, *Phys. Scr.* **2011**,*83*, 025604.
[50] Q. Wei, H. Liu, D. Wang, S. X. Liu, *Thin Solid Films.* **2011**,*519*, 5046.
[51] T. Wang, D. Zhao, M. Zhang, J. Yin, W. Song, Z. Jia, X. Wang, G. Qin, W. Qin, F. Wang, *Opt. Mater. Express.* **2015**,*5*, 469.
[52] H.-F. Li, X.-Q. Liu, C. Lyu, J. Gorbaciova, L.-L. Wen, G.-G. Shan, P. B. Wyatt, H.-Q. Ye, W. P. Gillin, *Light Sci. Appl.* **2020**,*9*, 32.
[53] D. K. Sardar, K. L. Nash, R. M. Yow, J. B. Gruber, *J. Appl. Phys.* **2007**,*101*, 113115.
[54] M. L. Zhang, G. J. Hu, S. R. Zhang, D. S. Gao, Y. D. Sun, F. Wang, *RSC Adv.* **2020**,*10*, 11148.
[55] Y. Yang, F. Wang, S. T. Ma, M. Zhou, Y. B. Lang, G. S. Qin, D. M. Zhang, W. P. Qin, D. Zhao, X. Zhang, *Polymer.* **2020**,*188*, 122104.
[56] G. Karve, B. Bihari, R. Chen, *Appl. Phys. Lett.* **2000**,*77*, 1253.
[57] J. Yang, M. B. Diemeer, G. Sengo, M. Pollnau, A. Driessen, *IEEE J. Quantum Electron.* **2010**,*46*, 1043.
[58] J. Yang, M. B. Diemeer, D. Geskus, G. Sengo, M. Pollnau, A. Driessen, *Opt. Lett.* **2009**,*34*, 473.
[59] D. Zhang, X. Li, X. Huang, S. Liu, H. Fu, K. Che, L. Wang, *IEEE Photonics J.* **2015**,*7*, 1400607.
[60] X. Yang, Z. Zhou, Y. Man, H. Xu, D. Zhang, *Chin. J. Lasers.* **2023**,*50*, 0601002.
[61] Y. Huang, Y. Man, G. Xie, C. Wang, B. Zhang, H. Xu, H. Fu, J. Zhu, Z. Lv, L. Ying, *Small Methods.* **2023**,*7*, 2201366.